2022 American Control Conference (ACC)
Atlanta, USA, June 8-10, 2022

A Novel Lightweight Cable-Driven Integrated-Finger Robotic Hand for Dexterous Manipulation

Xingsheng Wei[1], Kuiyuan Xu[1], Wansong Liu[1], Eric Mountain[1], Xiao Liang[2], and Minghui Zheng[1,*]

Abstract— **In recent years, the demands of using robotic hands have been increased dramatically in a variety of applications such as intelligent manufacturing. The current robotic hands usually are functioned relying on the assembly of numerous components, which bring unnecessary dead weight and complex control systems. Such shortcomings limit the further application of robotic hands. To address this issue, this paper presents a lightweight and low-complexity five-fingered robotic hand called the Integrated Finger Robotic Hand (IFRH). Each finger of the robotic hand is built as an integrated object based on a compliant joint called the Elastic Knuckle Connection (EKC). The 3D-printed finger design minimizes the number of components as well as the weight of the system. The IFRH can be assembled quickly and maintained easily due to its low number of parts compared to traditional separate-finger robotic hands. The IFRH is driven by servo motors which transmit motion to a monofilament fishing string. This fishing string is connected to each finger, which mirrors the grasping motion of a real human hand when contracted. With feedback from force sensors, the IFRH accomplishes the goal of high precision grasping of daily objects. The IFRH can be controlled by a potentiometer powered by Arduino, further increasing the user-friendly nature of the robotic hand. A number of experimental tests are conducted to verify the accuracy of the force transmission system, the grasping capabilities, and the grasping precision.**

I. INTRODUCTION

The robotic hand field is ever broadening due to its high demand for various applications such as intelligent manufacturing and remanufacturing [1]–[4]. The common elements of a robotic hand are to mimic the functionality of a human hand while maintaining light weight, low cost, and ease of use. Tian et al. [5] created the Nadine hand, which mimics the human hand by use of cable-driven fingers. Cabás et al. [6] designed the RL1 hand, which can be controlled by simple commands sent from a computer. Devi et al. [7] developed a flexible actuator as a bending joint on a robotic hand. This allows the hand to be both lightweight and flexible.

Whether it is for structural design, programming, or control of the robotic hand, its functionality needs to meet the grasping demands of common household objects. Other robotic hands with higher grasping precision may be able to perform tasks that the IFRH cannot, such as holding an object double its weight or writing with a pen/pencil. One robotic hand with high grasping precision is the iLimb, analyzed by Betler et al. [8]. The fingers of the iLimb hand contain a series of small motors and metal gears attached to fibrous cables. The pulling of these cables drives the grasping of all five fingers. The iLimb is able to grasp with a wide range of motion at a speed of 200 mm/s. Another example of a high precision grasping robotic hand is the Dextrus hand, analyzed by Phillips et al. [9]. The Dextrus hand possesses fingers with individual joints that are reinforced with steel. The number of individual joints corresponds to the that of a human hand, which aids in the Dextrus hand's ability to closely wrap each finger around an object.

Since the average weight of a real human hand is roughly 400 grams [10], prosthetic designs exceeding that threshold can be a burden to human beings. Xu et al. [11] created a biomimetic robotic hand that weighs 942 grams. Medynski et al. [12] designed a myo-electric hand with preset grip positions, weighing 550 grams. The next lightest robotic hand design is the Nadine hand created by Tian et al. [5], which is also 3D-printed and weighs in at 150 grams. The Nadine hand requires 6 actuators to operate and is unable to calculate the tip force of each finger while grasping an object.

Different robotic hands have varying levels of ease of use, depending on the hand's complexity. For instance, the tendon-driven three-finger robotic hand moves its fingers by use of an RC servo motor and an additional DC motor in [13]. Therefore, two motor driven forces must be input to function the hand. Another complex design is the biomimetic hand created by Xu et al. [11]. The hand operates by observing the motion of a human operator, calculating the kinematics, and performing the operation to the best of its ability. This level of complexity requires knowledge of intricate feedback loops and biomimetics. Furthermore, Gaiser et al. [14] presents a new anthropomorphic robotic design which utilizes multiple sensors to control its grasping operations. The hand collects, interprets, and transmits data from angle, pressure, and tactile sensors. This high volume of input data increases the accuracy of the hand's movements, but also increases its difficulty of use.

To determine when the hand should cease grasping, a force sensor is required. The iLimb and Bebionic hands [8] each use two force sensors to know when to halt the grasping process. The combination of force sensors attempt to simulate the muscle's response to nerve stimulation.

This work was supported by the USA National Science Foundation under Grant No. 2132923.

[1] Xingsheng Wei, Kuiyuan Xu, Wansong Liu, Eric Mountain, and Minghui Zheng are with the Department of Mechanical and Aerospace Engineering, University at Buffalo, Buffalo, NY14260, USA. Emails:{xwei9, kuiyuanx, wansongl, ericmoun, mhzheng}@buffalo.edu.

[2] Xiao Liang is with the Department of Civil, Structural and Environmental Engineering , University at Buffalo, Buffalo, NY14260, USA. Email:liangx@buffalo.edu.

[*] Corresponding Author.

Crisman et al. [15] also presents a multi sensor design for the Graspar hand. A switch sensor is located in each fingertip, totaling five sensors in the hand. While the switch sensors are inexpensive, they do not provide detailed information (especially when grasping an object with a large length to diameter ratio). The IFRH stands out in this case since it only requires one force sensor. This again reduces the cost and weight of the hand while maintaining ease of use. Phillips et al. [9] researches myoelectric prostheses for general applications. These prosthetic use electromygraphy sensors to communicate electric signals to the motors. These sensors, although very accurate, only function on extremely clean surfaces and can only be used once.

While the IFRH may have a lower grasping precision in relation to other robotic hands, its simplified design reduces weight and cost compared to the high precision designs. Furthermore, the IFRH weighs the least out of all other robotic hands compared in this paper, at 125 grams. This light weight is made possible by the IFRH's 3D-printed EKC, which utilizes the high tensile strength and elastic properties of PLA [16]. This design is able to replace the function of pin connections and springs in the fingers, which also reduces the hand's cost. Additionally, the IFRH does not reproduce the over 15 degrees of freedom (DOF) of a human hand. Another key advantage of the IFRH is its ease of control compared to traditional separate-finger robotic hands. This user friendly function is made possible from the limited number of sensors, actuators, and DOF of the overall hand. Finally, the IFRH only requires one force input for its servo motor, compared to other robotic hand models, which require multiple data inputs. Force-dependent controlling systems are superior to time-dependent controlling systems for our applications since we do not always know the size of the object that is being grasped.

The paper is organized as follows. Section II introduces design details and developments of the IFRH. The related simulations and experimental tests of the IFRH are demonstrated in Section III. Finally, Section IV concludes the paper.

II. DESIGN

The traditional robotic hand's fingers tend to treat the knuckles of the fingers as separate components, i.e., the under-actuated robotic hand [6], the bionic hand [11], and the humanoid robotic hand [5]. Even though the shapes of these separate-finger robotic hands are similar to real human hands, the current robotic hands consist of large numbers of similar phalanges, connection, and transmission components (pins, gears, springs, and pulleys). These components do not only introduce unwanted dead weight to the whole system but also increase the design complexity, cost, and difficulty of controlling the product. This limits the application of robotic hands in the civilian field. To expand the application field of robotic hands, a simpler design with a lighter weight is required.

The IFRH's design focuses on the imitation of real hands. Actually, a complete reproduction of the real human hand requires high cost and complex design since the real hand has enough DOF to ensure its functionality. Therefore, to satisfy the balance between functionality and weight, the IFRH is designed with five DOF. The following subsections introduce the knuckle and force-transmission system designs, the sensor selection, and the control algorithm.

A. Design of Integrated Fingers

The core design of the integrated finger is the Elastic Knuckle Connection (EKC) shown in Fig. 1. It functions as not only a connection between phalanges of fingers but also a storage of elastic energy when the finger bends. The stored energy is the source of the pull-back force to reset the fingers. In another word, the EKC serves as the combination of pin connection between the phalanges of fingers and the pull-back spring of traditional tendon fingers.

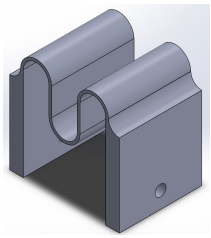

Fig. 1. 3D modeling of the Elastic Knuckle Connection (EKC)

The thumb of the IFRH is designed with two knuckles, and the other four fingers are designed with three knuckles. The 3D models of the thumb and forefinger are shown in Fig. 2 and Fig. 3 as examples. In a real human hand, the first joint of the thumb, where the thumb connects the palm, has two DOF. The design of the IFRH compromised the two DOF into one. For the other fingers, the connection to the palm has a pinhole to allow a little bit of rotation of 0-10 degrees. This makes the hand fit better when grasping objects of different shape.

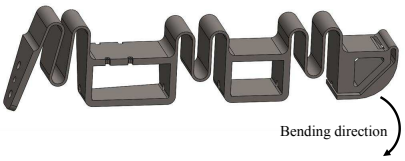

Fig. 2. 3D modeling of the thumb

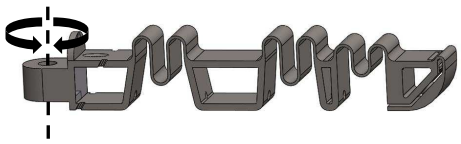

Fig. 3. 3D modeling of the forefinger

B. Design of Force-Transmission System

Right now, the available force-transmission systems are tendons with springs [13], hydraulic pressure [14], or pulley-idler unit [15]. These different systems are able to transmit

the torque from the motor to the force driving the fingers to move to the desired position. They usually introduce a large amount of dead weight to the robotic hand and require maintenance during usage, especially for the hydraulic pressure system. To save weight, this paper uses monofilament fishing string as a simple yet efficient force-transmission object to bend and release fingers of the IFRH.

The string traveling through the designed holes serves as the replacement of the above-mentioned force-transmission system shown in Fig. 4. The end of the string is connected to the fingertip, and the start of the string is connected to a servo motor. The string is controlled by the servo motor and served as the converter between motor torque and finger-bending force. For example, the string's length will be shortened with the clockwise rotating motor, and this decrease in length will force the finger to bend. The finger can be reset with a counterclockwise rotating motor.

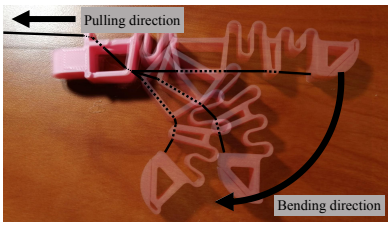

Fig. 4. Transmission of IFRH

C. Sensor and Control

Since it's difficult to predict the bending time of the finger for an unknown object, we choose a force-dependent controlling system instead of a time-dependent controlling system in this study. To enable the IFRH to grasp different kinds of objects successfully, the contact force acting on the fingers of the IFRH must be obtained by a sensor. Considering the weight, cost, and sensitivity of the sensor, we choose the force-sensitive resistor (FSR) to estimate the reaction force from the fingertips in this study. The measurement range of the FSR sensor is from 0 to $19.62N$. The FSR sensor shape and the sensing area of 40 mm^2 are shown in Fig. 5. The FSR sensor is installed into a slit of the IFRH fingertip as illustrated in Fig. 6. The outer flexible layer first compresses the FSR's sensing area when it is applied by a force. Next, the sensor provides electrical signals based on the applied force [17]. Finally, the electrical signal is used as grasping feedback to control the servo such that the grasping process can be completed.

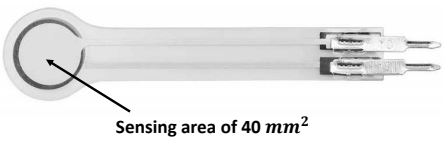

Fig. 5. Sensing shape and area of the FSR

To grasp objects smoothly, a proportional-integral (PI) controller to reduce the amplitude of the finger's oscillation is

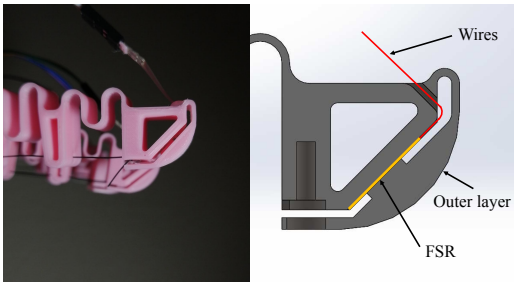

Fig. 6. Fingertip and section view

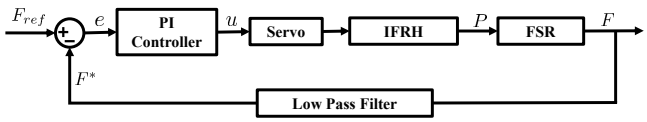

Fig. 7. Flow chart of controlling

utilized. The framework of the control flow is demonstrated in Fig. 7. F_{ref} is a reference contact force defined by users. The value of F_{ref} depends on the maximum torque output of the servo motor and the grasped objects. The reading contact force of the FSR sensor is denoted as F_k, where the subscript k in this paper denotes the time step. The force from sensor F_k first goes through a low-pass filter to cancel the unwanted high-frequency noise to obtain F_k^*. Then, the filtered sensor force F_k^* works as negative feedback to generate error e_k with the following equation:

$$e_k = F_{ref} - F_k^* \tag{1}$$

The error is the input to the PI controller. The PI controller generates the control signal u_k using the following equation:

$$u_k = K_p e_k + K_i \int_0^k e_k \tag{2}$$

where K_p and K_i are two user-defined parameters. The output of the PI controller is a control signal to control the servo motor such that the finger is able to bend. The finger's position P_k is updated using the following equation:

$$P_k = P_{k-1} + g(u_k) \tag{3}$$

where $g(\cdot)$ is a mapping function from the control signal to the movement of the finger's bending through the servo. As the finger of the IFRH is bending, the force from the FSR sensor F_k is filtered with the following equation:

$$F_k^* = F_{k-1}^* + \omega(F_k - F_{k-1}^*)dt \tag{4}$$

where ω is the cut-off frequency and dt is the sampling time. The filtered force reading F^* is combined adversely with F_{ref} and sent out as e to be executed in the next time step.

The integrated finger is advantageous because its control is much straighter and easier compared to traditional separate-finger robotic hands. For instance, Sung-Yoon Jung's tendon-driven three-finger robotic hand [13] moves its finger under the drive of an RC-servo motor and an extra DC motor. Traveling through wires, the force from the motors changes the

finger's position with the help of two pulleys, an metacarpo phalangeal joint, and a proximal interphalangeal joint. For its control, it is necessary to put two motors' driven forces, positions of the above-mentioned pulleys and joints, and the link between the joints into consideration. Things change when considering the IFRH's control. As shown in Fig. 7, with the selected ω=500rad/ms, dt=1ms, K_p=0.01, and K_i=0.1, the IFRH only needs one force input as a reference for the servo motor to drive the finger to a position where the sensor's reading meets the reference. The single motor controlling of each finger and the compliant nature of the IFRH also allows a lower accuracy in control while fitting well around the object that is being grasped.

III. Simulation and Experimental Tests

A. Simulation

This subsection presents numerical studies to validate the effectiveness of the developed robotic hand. The aim of developing the IFRH is to mimic the movement of a real human hand. Fig. 8 and Fig. 9 show the bending of the real human finger and the IFRH finger respectively. To better compare the knuckle changes between the IFRH and a real human finger, θ_i and θ_i' are denoted as the joint angles of the IFRH and human fingers respectively, where i stands for the number of the finger joints. ΔL stands for the pulled distance of the force-transmitting fishing string. L_0' represents the inside length of the figure before bending, L' stands for the inside length of the finger after bending, and $\Delta L'$ denotes the inside length change.

In summary, the following variables are used to describe the grasp tracking.

- θ_1 is the angle of the first EKC.
- θ_2 is the angle of the second EKC.
- θ_3 is the angle of the third EKC.
- ΔL is the pulled distance of the string.
- θ_1' is the angle of the first human finger joint.
- θ_2' is the angle of the second human finger joint.
- θ_3' is the angle of the third human finger joint.
- $\Delta L'$ is the changed inside length of the human finger.

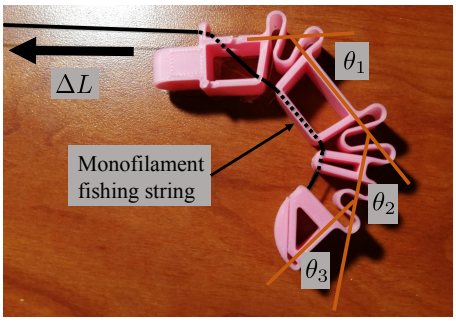

Fig. 8. Definitions of variables of the robotic finger

To enable the bending of the IFRH finger to be similar to the bending of the real human finger, we simulate the case of applying force on the EKC in SOLIDWORKS software, and modify the design of the EKC such that the finger

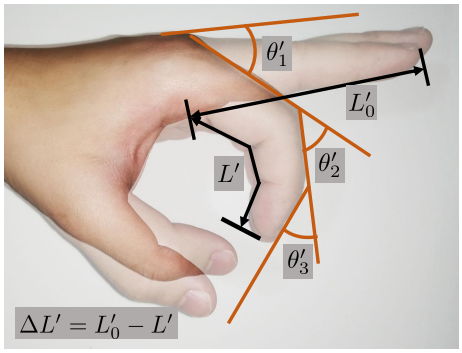

Fig. 9. Definition of variables of the human finger

can approach the desired bending angle. When the IFRH finger is bending, the only applied force is the force acting along the monofilament fishing string. The only relatively moving surfaces are the smooth outside surface of the fishing string and the inside holes of the fingers. To simplify the problem and considering monofilament fishing string has a smooth surface, friction during the bending is ignored in the simulation. The simulation setting demo of EKC is presented in Fig. 10. One side of the EKC is fixed, and another side is applied with a 0.5 N driving force. The hue of the EKC demo represents the degree of deflection labeled URES which is a static displacement plot. α denotes the deflection angle of the EKC side. α can be changed by modifying the design of the EKC such that the IFRH finger's bending is close to a real finger's bending.

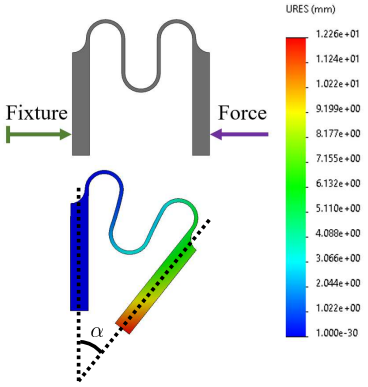

Fig. 10. EKC simulation setting and result

To demonstrate the imitation performance of the IFRH, a comparison between the IFRH finger and the human finger has been developed. Considering the forefinger has the same movement as other fingers except for the thumb, the forefinger is used to model the grasping tracking. Suppose that the human hand and the IFRH grasp the same object. The inside length change sequence of the human finger during such grasping is denoted as $\Delta\mathcal{L}' = [\Delta L_0', \ldots, \Delta L_{M-1}']$, where M is the total number of steps. The corresponding human finger joint angles are first recorded. Next, the fishing string of the IFRH finger is pulled with M steps to grab the

object, the pulled distance sequence of the string is denoted as $\Delta\mathcal{L} = [\Delta L_0, \ldots, \Delta L_{M-1}]$, and the corresponding IFRH finger joint angles are recorded as well. Finally, the joint angle comparison of bending tracking between the real forefinger and the IFRH forefinger is demonstrated in Fig. 11.

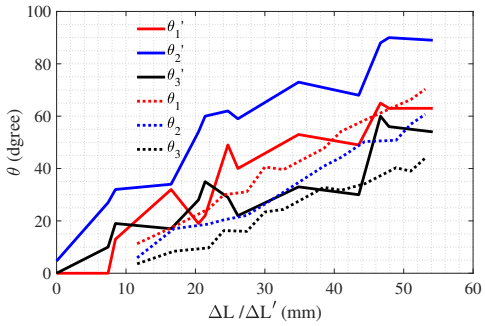

Fig. 11. Joint angle comparison of bending between the human finger and IFRH finger

TABLE I
LINEAR REGRESSION EQUATION'S SLOPE COMPARISON

	θ_1' vs θ_1		θ_2' vs θ_2		θ_3' vs θ_3	
	Slope	Error	Slope	Error	Slope	Error
Real	6.5054	NA	5.7033	NA	4.1429	NA
Sim	4.9038	0.2462	4.4225	0.2246	3.3643	0.1879

We also calculate the linear regression equations for the lines shown in Fig. 11. The corresponding equations' slopes of the knuckles are compared in Table I to evaluate how close the moving track of the IFRH's forefinger is to the real one's. It clearly shows that the simulated integrated forefinger behaves similarly to a real human hand. Considering the performance of the simulated IFRH in Fig. 11, there is the possibility that the measurements of $\Delta L'$ and θ_i' have errors, especially for θ_2'. One possible reason for the discrepancy is that human finger data are measured based on a film which we think would decrease the effect of uncontrollable shaking of the finger during measurement. It seems that the distortion of the camera lens introduces more deviation than we anticipated. The middle phalange is relatively shorter which would require the second EKC to rotate more, hence amplifying the differences between it and the real hand's middle phalange.

B. Experimental tests

After the assembly, the whole appearance of the IFRH is shown in Fig. 13. The length, width, and height of the assembled IFRH are 200mm, 60mm, and 30mm, respectively, which is similar to a real human hand. As expected, the whole IFRH's weight is 125 grams (including motors, sensors, wires, screws, and glue, excluding the motor driver board, the micro-controller, and the tube where the hand-mounted on), which is significantly lighter than current other kinds of robotic hands. The overall weight of the IFRH proves the accomplishment of its weight reduction goal. The weight comparisons of the IFRH to other modern robotic hands are shown in Table III. It is clear that the weight reduction is significant. With an ensured grasping capability, the whole system's weight is now the lightest and significantly lighter than the second lightest one, Nadine hand, which also uses 3D-printed parts.

TABLE II
WEIGHT COMPARISON OF SEVERAL ROBOTIC HANDS

Robotic hand name	Mass (g)
Integrated-Finger Robotic Hand	125
Nadine hand [5]	150
Tact Hand [10]	350
InMoov [18]	400
Dextrus [9]	428
i-Limb [8]	460 - 465
Bebionic [12]	550
Zhe Xu hand [11]	942

With six separate main components, five micro-servos, five FSR, and about 30 pieces of small accessories (M2 screws, fishing strings, and wires), the IFRH can be assembled within 30 minutes. Furthermore, the integrated finger can be replaced easily when encountering any unexpected damage. Its maintenance is surprisingly simple especially compared with the hydraulic ones.

The IFRH was tested grasping a range of daily tools and foods to show its capabilities. From light paper towels to a fragile egg; from a heavy round screw driver to a square screw box, the IFRH shows its ability to deal with a wide range of tasks. As the discussed control framework for the current IFRH, the most critical part is the preset input force F_{ref}, as it determines the output force F which is applied on the object being grasped. A relatively small F_{ref} will be chosen when dealing with light and fragile objects such as eggs or oranges, and a larger F_{ref} will be chosen for heavier objects such as the screw driver. The fingers fit the shape of the objects depending more so on the sensor when F_{ref} is set smaller. However, the fingers fit the shape of objects more on the compliance of the fingers when F_{ref} is set larger. Fig. 12 displays the grasped samples and Table. III provides the samples' weights.

TABLE III
WEIGHTS OF GRASPED SAMPLES

Sample	Weight [g]
Cutter	51
Egg	60
Screw Driver	97
Paper Towel	106
Screw Box	180
Bottle Water	215

As shown above, the IFRH can handle the majority of daily tasks. In another word, its working range covers the desired goal. It should be admitted that other robotic hands

Fig. 12. Demonstration of grasping capabilities: (a) Grab of cutter; (b) Grab of egg; (c) Grab of screw driver; (d) Grab of paper towel; (e) Grab of screw box; (f) Grab of bottle water

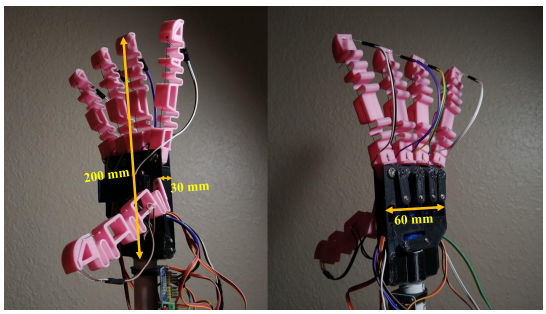

Fig. 13. The whole appearance of the Robotic Hand

can handle some tasks which the current IFRH cannot handle. Due to the sole DOF of each finger, and the limited capacity of micro-servos, the current IFRH cannot perform tasks with very high precision or heavy loads, such as writing with a pen or holding a weight double itself. However, based on the lightweight, low cost, simple structure, and high efficiency of force transmission, the IFRH can find its position in other applications.

IV. CONCLUSIONS

This paper introduced a simple yet effective Integrated-Finger Robotic Hand. The 3D-printed fingers and palm assist IFRH to have a lightweight of 125 grams. The string-based force-transmission system provides a simple way to control the bending motion of the IFRH. The primary application platform of the IFRH is the civilian field as that is the design focus of the project. Taking its grasping performance into consideration, it is fair to say the IFRH has a significant advantage of acceptable everyday performance. The functionality of the IFRH is worth further research to assist civilians around the world.

REFERENCES

[1] Meng-Lun Lee, Sara Behdad, Xiao Liang, and Minghui Zheng. A real-time receding horizon sequence planner for disassembly in a human-robot collaboration setting. In *2020 International Symposium on Flexible Automation (ISFA)*, 2020.

[2] Meng-Lun Lee, Sara Behdad, Xiao Liang, and Minghui Zheng. Disassembly sequence planning considering human-robot collaboration. In *2020 American Control Conference (ACC)*, pages 2438–2443. IEEE, 2020.

[3] Meng-Lun Lee, Sara Behdad, Xiao Liang, and Minghui Zheng. Task allocation and planning for product disassembly with human–robot collaboration. *Robotics and Computer-Integrated Manufacturing*, 76:102306, 2022.

[4] Seyedomid Sajedi, Wansong Liu, Kareem Eltouny, Sara Behdad, Minghui Zheng, and Xiao Liang. Uncertainty-assisted image-processing for human-robot close collaboration. *IEEE Robotics and Automation Letters*, 7(2):4236–4243, 2022.

[5] Li Tian, Nadia Magnenat Thalmann, Daniel Thalmann, and Jianmin Zheng. The making of a 3d-printed, cable-driven, single-model, lightweight humanoid robotic hand. *Frontiers in Robotics and AI*, 4:65, 2017.

[6] Ramiro Cabás, Luis Maria Cabas, and Carlos Balaguer. Optimized design of the underactuated robotic hand. In *Proceedings 2006 IEEE International Conference on Robotics and Automation, 2006. ICRA 2006.*, pages 982–987. IEEE, 2006.

[7] Mata Amritanandamayi Devi, Ganesha Udupa, and Pramod Sreedharan. A novel underactuated multi-fingered soft robotic hand for prosthetic application. *Robotics and Autonomous Systems*, 100:267–277, 2018.

[8] Joseph T Belter, Jacob L Segil, and BS SM. Mechanical design and performance specifications of anthropomorphic prosthetic hands: a review. *Journal of rehabilitation research and development*, 50(5):599, 2013.

[9] Brienna Phillips, Gabrielle Zingalis, Sarah Ritter, and Khanjan Mehta. A review of current upper-limb prostheses for resource constrained settings. In *2015 IEEE global humanitarian technology conference (GHTC)*, pages 52–58. IEEE, 2015.

[10] Patrick Slade, Aadeel Akhtar, Mary Nguyen, and Timothy Bretl. Tact: Design and performance of an open-source, affordable, myoelectric prosthetic hand. In *2015 IEEE International Conference on Robotics and Automation (ICRA)*, pages 6451–6456. IEEE, 2015.

[11] Zhe Xu and Emanuel Todorov. Design of a highly biomimetic anthropomorphic robotic hand towards artificial limb regeneration. In *2016 IEEE International Conference on Robotics and Automation (ICRA)*, pages 3485–3492. IEEE, 2016.

[12] Courtney Medynski and Bruce Rattray. Bebionic prosthetic design. In *Myoelectric Symposium*, 2011.

[13] Sung-Yoon Jung, Sung-kyun Kang, Myoung-Jun Lee, and Inhyuk Moon. Design of robotic hand with tendon-driven three fingers. In *2007 International Conference on Control, Automation and Systems*, pages 83–86. IEEE, 2007.

[14] Immanuel Gaiser, Stefan Schulz, Artem Kargov, Heinrich Klosek, Alexander Bierbaum, Christian Pylatiuk, Reinhold Oberle, Tino Werner, Tamim Asfour, Georg Bretthauer, et al. A new anthropomorphic robotic hand. In *Humanoids 2008-8th IEEE-RAS International Conference on Humanoid Robots*, pages 418–422. IEEE, 2008.

[15] Jill D Crisman, Chaitanya Kanojia, and Ibrahim Zeid. Graspar: A flexible, easily controllable robotic hand. *IEEE Robotics & Automation Magazine*, 3(2):32–38, 1996.

[16] Yu Zhao, Yuansong Chen, and Yongjun Zhou. Novel mechanical models of tensile strength and elastic property of fdm am pla materials: Experimental and theoretical analyses. *Materials & Design*, 181:108089, 2019.

[17] Ahmed M Almassri, WZ Wan Hasan, Siti Anom Ahmad, Asnor J Ishak, AM Ghazali, DN Talib, and Chikamune Wada. Pressure sensor: state of the art, design, and application for robotic hand. *Journal of Sensors*, 2015, 2015.

[18] Gael Langevin. Inmoov-open source 3d printed life-size robot. *pp. URL: http://inmoov. fr, License: http://creativecommons. org/licenses/by–nc/3.0/legalcode*, 2014.